

Mooring-Based Observations of Double-Diffusive Staircases over the Laptev Sea Slope*

IGOR V. POLYAKOV, ANDREY V. PNYUSHKOV, ROBERT REMBER, AND VLADIMIR V. IVANOV

International Arctic Research Center, University of Alaska Fairbanks, Fairbanks, Alaska

Y.-D. LENN

School of Ocean Sciences, Bangor University, Menai Bridge, United Kingdom

LAURIE PADMAN

Earth & Space Research, Corvallis, Oregon

EDDY C. CARMACK

Fisheries and Oceans Canada, Institute of Ocean Sciences, Sidney, British Columbia, Canada

(Manuscript received 18 October 2010, in final form 8 September 2011)

ABSTRACT

A yearlong time series from mooring-based high-resolution profiles of water temperature and salinity from the Laptev Sea slope (2003–04; 2686-m depth; 78°26'N, 125°37'E) shows six remarkably persistent staircase layers in the depth range of ~140–350 m encompassing the upper Atlantic Water (AW) and lower halocline. Despite frequent displacement of isopycnal surfaces by internal waves and eddies and two strong AW warming pulses that passed through the mooring location in February and late August 2004, the layers preserved their properties. Using laboratory-derived flux laws for diffusive convection, the authors estimate the time-averaged diapycnal heat fluxes across the four shallower layers overlying the AW core to be ~8 W m⁻². Temporal variability of these fluxes is strong, with standard deviations of ~3–7 W m⁻². These fluxes provide a means for effective transfer of AW heat upward over more than a 100-m depth range toward the upper halocline. These findings suggest that double diffusion is an important mechanism influencing the oceanic heat fluxes that help determine the state of Arctic sea ice.

1. Introduction

Over the past two decades the steady warming of the Arctic Ocean interior was interrupted by two large-scale, warm, pulse-like events. The first evidence of a warming event spreading in the intermediate (depth range of ~150–900 m) Atlantic Water (AW; potential temperature $\theta > 0^{\circ}\text{C}$) layer of the Arctic Ocean was found in the Eurasian Basin in 1990 (Quadfasel et al. 1991) and in the Canadian Basin in 1993 (Carmack et al. 1995). Another

pulse of warm water entered the Arctic Ocean interior through Fram Strait in the early 2000s (e.g., Schauer et al. 2004; Polyakov et al. 2005; Dmitrenko et al. 2008). The AW is carried into the Arctic Ocean interior by the pan-Arctic boundary current (e.g., Aagaard 1989; Rudels et al. 1994). This system provides the largest inputs of water, heat, and salt into the Arctic Ocean; the total quantity of heat is huge, enough to melt the Arctic ice cap several times over.

The AW is believed to be effectively insulated from the pack ice and atmosphere by a cap of fresh, cold surface water bounded below by a strong pycnocline (e.g., Rudels et al. 1996) in which salinity increases from near-surface values of 33 or lower to around 34.5 at 150–300-m depth. At the same time, the decrease of AW temperature with increasing distance from Fram Strait implies that AW heat must be lost as the AW spreads. Much of this heat is spread laterally by advection, eddy stirring, or other processes, but some portion is lost upward to the overlying

* ESR Publication Number 144.

Corresponding author address: Igor V. Polyakov, University of Alaska Fairbanks, International Arctic Research Center, 930 Koyukuk Drive, Fairbanks, AK 99775.
E-mail: igor@iarc.uaf.edu

halocline waters (e.g., Rudels et al. 1996; Steele and Boyd 1998; Martinson and Steele 2001; Polyakov et al. 2010).

The few available turbulence estimates based on microstructure observations suggest very small diffusivities, less than $\sim 10^{-5} \text{ m}^2 \text{ s}^{-1}$ in the Arctic Ocean interior, away from topographic boundaries (e.g., Rainville and Winsor 2008; Fer 2009). The resulting turbulent heat fluxes from the AW layer are also small, less than 1 W m^{-2} . However, fluxes can vary over a wide range depending on geographical location and depth. For example, heat fluxes in the Canada Basin at the base of the mixed layer and near the ice base were estimated to be $0.3\text{--}1.2 \text{ W m}^{-2}$ and 0.2 W m^{-2} , respectively, whereas higher estimates of $2.1\text{--}3.7 \text{ W m}^{-2}$ (mixed layer) and 3.5 W m^{-2} (below ice) were obtained over the Chukchi Borderlands (Shaw et al. 2009). In the vicinity of the Yermak Plateau, the vertical eddy diffusivity was estimated to be $\sim 2.5 \times 10^{-4} \text{ m}^2 \text{ s}^{-1}$ in the pycnocline, implying an upward heat flux of $\sim 25 \text{ W m}^{-2}$ (Padman and Dillon 1991).

Published estimates of fluxes at the ocean surface, dominated by summer solar heat uptake and subsequent release of that heat in winter to the atmosphere and ice formation, are much higher than those in the ocean interior (e.g., Maykut and McPhee 1995; McPhee et al. 2003; Krishfield and Perovich 2005; Shaw et al. 2009). For example, enhanced upper-ocean solar heating through leads and consequent strong [$O(100) \text{ W m}^{-2}$] heat fluxes and ice bottom melting were found in the Beaufort Sea in summer 2007 (Perovich et al. 2007, 2008; Toole et al. 2010). Recently, Sirevaag and Fer (2009), using observations from north of Svalbard, found heat fluxes of $O(100) \text{ W m}^{-2}$ at the ice–ocean interface within the branches of the West Spitsbergen Current. However, even though the instantaneous ocean–atmosphere heat exchange exceeds time-averaged interior ocean heat fluxes by two orders of magnitude, the interior heat flux is a significant fraction of the annual-averaged heat budget for the surface mixed layer and sea ice thermodynamic balances. Thus, in order to assess the interannual response of the Arctic sea ice, we need to accurately quantify the upper-ocean fluxes due to processes that are not directly related to ocean surface heat, freshwater, and momentum exchanges.

The most important mechanisms for diapycnal transport in the Arctic Ocean are shear-driven instabilities and double diffusion (for a review, see Padman 1995). In the present study, we focus on double diffusion because our data, from the continental slope of the Laptev Sea, show ubiquitous layers of near-uniform potential temperature θ and salinity S separated by strong-gradient, relatively thin interfaces (or “sheets”). These “thermohaline staircases” are assumed to arise through the effect of the different molecular diffusivities of heat and salt (Turner 1973) and are found over a large portion of the Arctic

Ocean (e.g., Timmermans et al. 2008). The so-called diffusive instability (or “diffusive convection”) mode of double diffusion is found where cold and freshwater lies above warm and salty water, typically above the depth of maximum θ in the AW layer. Padman and Dillon (1987, 1989) used data from microstructure profiles to estimate double-diffusive heat fluxes in the range of $0.02\text{--}0.1 \text{ W m}^{-2}$ above the AW core (320–430 m) in the Canada Basin. Timmermans et al. (2008) estimated similar values based on ice-tethered profiler data and laboratory-based double-diffusive flux “laws.” Lenn et al. (2009) used concurrent measurements of turbulent dissipation and temperature–salinity fine structure to estimate vertical double-diffusive heat fluxes of $\sim 1 \text{ W m}^{-2}$ and stronger along the eastern Eurasian Basin boundary. The same authors estimated that turbulent kinetic energy dissipation associated with shear instability in the 100–250-m layer is too weak to overcome the existing background stratification; hence, double-diffusive convection may be the primary diapycnal mixing mechanism in that region.

Based on these prior observations, we identify a need for better understanding of Arctic double-diffusive processes and their temporal variability. In this paper, we report on an approximately one-year time series of hydrographic and velocity profiles obtained from a mooring deployed on the continental slope of the Laptev Sea (section 2). We then describe the thermohaline staircase characteristics seen in this dataset (section 3) and estimate the associated upward heat fluxes above the AW core (section 4). Section 5 discusses implications of our measurements for general representation of diffusive layer (DL) staircases, including the possibility that externally imposed shear from mean flow or tides may modify the estimated vertical fluxes. We present our principal conclusions in section 6.

2. Observational data

The data used in this study were collected from a mooring deployed on the Laptev Sea continental slope (Fig. 1). Mooring M1 ($78^{\circ}26'N$, $125^{\circ}37'E$) collected data over several years; however, for this study we used data collected in 2003–04 only (the year with the most complete data record) because of the highly labor-intensive procedures involved in the data processing and analysis. The 2004–05 record (not shown) also shows fine structure that is similar to that found in the 2003–04 record. The mooring was equipped with a McLane moored profiler (MMP), which includes a conductivity–temperature–depth (CTD) sensor and an acoustic current meter (ACM). The MMP sampled a vertical profile along a mooring line at a speed of $\sim 25 \text{ cm s}^{-1}$ with a sampling period of 0.5 s; therefore, the raw data had a vertical spacing of $\sim 12 \text{ cm}$. The

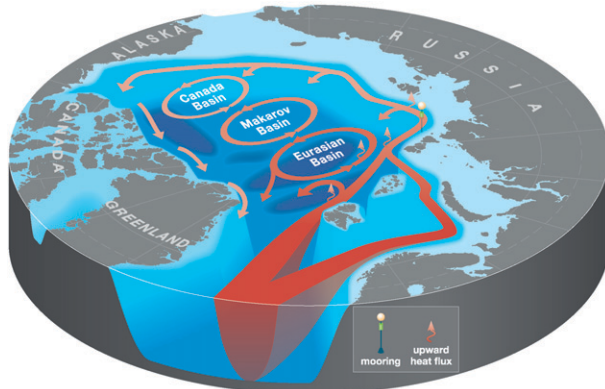


FIG. 1. Circulation of the intermediate AW of the Arctic Ocean shown by red and pink arrows. In the real ocean, the flows likely follow topographic slopes; the arrows show schematic pathways and do not reflect details of the flow. The mooring position in the eastern Eurasian Basin is indicated.

2003–04 deployment provided yearlong daily CTD and velocity records between 105 and 1509 db. In the analysis, we used data interpolated to a 15-cm fixed vertical grid; that is, close to the original sampling interval.

The MMP carried a Falmouth Scientific, Inc. (FSI) microCTD sensor in 2002–04 and a Sea-Bird Electronics (SBE) 41CP CTD sensor in 2004–05, with temperature and conductivity measurement accuracies for T and C of about $\pm 0.002^\circ\text{C}$ and $\pm 0.0002 \text{ S m}^{-1}$, respectively. The velocity precision and resolution of the FSI ACM carried on the MMP are reported to be $\pm 3\%$ of reading and $\pm 0.01 \text{ cm s}^{-1}$, respectively. Compass accuracy is $\pm 2^\circ$. All MMP sensors were calibrated before their deployment and immediately after their recovery using McLane facilities.

3. Staircase characteristics

a. Identification and definition of interfaces

Time series of θ , S , and potential density σ_θ profiles derived from the MMP record (Fig. 2, left) show that strong warming signals were advected to the mooring site from upstream locations in the form of pulse-like anomalies in February and late August 2004 (for details, see Polyakov et al. 2005, 2010, 2011). Corresponding increases in S partially compensated for the effects of warming on changes in density stratification; the compensation, however, was not complete, so the warming correlated with a σ_θ decrease in the AW layer expressed as a substantial (tens of meters) descent of isopycnal surfaces (Fig. 2, left).

The daily profiles were used to derive θ , S , and σ_θ anomalies, which were taken relative to vertical means calculated within a 3-m running window. An example profile of mean and anomalous $\theta(z)$ and $S(z)$ (Fig. 3) shows a vertical sequence of quasi-homogeneous layers in the

upper (above ~ 220 m) portion, separated by interfaces (or sheets) in which vertical gradients of θ and S are relatively large; we refer to this structure as a double-diffusive (or thermohaline) staircase. The local maxima of successive anomalies in θ and S define the boundaries of the strong-gradient interfaces (Fig. 3). This association was used to identify the depths of the upper and lower boundaries of the interfaces (Fig. 4). Changing the width of the vertical window used to define vertical means does not change the depth of the local maxima; it just changes the strength of anomalies (not shown). Thus, this algorithm is robust in identifying the interface boundaries. Note that the algorithm does not depend on a priori assumptions, such as a threshold of $\partial\theta/\partial z = 0.005^\circ\text{C m}^{-1}$ used by Timmermans et al. (2008), for interface detection.

Using this algorithm, we identified six strong-gradient continuous interfaces: the shallowest one is located at ~ 160 m and the deepest one is located at ~ 300 m (Fig. 2, right). The boundaries of the interfaces identified by the algorithm were verified using visual inspection of the vertical profiles of θ and S . The interfaces in the lower halocline and upper AW layer (~ 150 – 350 m) are continuous throughout the entire 2003–04 record (Fig. 2); they can also be found in the 2004–05 record (not shown). Continuous interfaces above 160 m and below 350 m were difficult to identify because of intensive merging and splitting of interfaces, a process that often caused interfaces to lose their identity (merging of the upper two selected interfaces during the second half of the record is expressed as gaps in the layer depths and can be seen, e.g., in Fig. 4). We note also that the strength of the θ and, in particular, the S anomalies used to identify the interfaces decrease in the upper halocline (shallower than 150 m; not shown) and in the deeper part of the AW layer (deeper than 350 m); analysis of the staircase structure in these parts of the water column is difficult.

b. Vertical displacements of interfaces

Large vertical displacements of the interfaces are evident from Fig. 4; they are roughly correlated with perturbations of the isopycnal surfaces (see Fig. 2, bottom left) and the depth of maximum AW temperature. Particularly strong vertical displacement of isopycnal surfaces was observed during the warming events in February and late August 2004, when the lowering of the two lowest layers exceeded 50 m (Fig. 4). The θ - S diagram shows gradual warming, salinization, and lightening of all interfaces associated with long-term water-mass changes (Fig. 5).

The staircase structure within the ~ 150 – 250 -m depth range is generally robust. For example, eddy-like features passing through the mooring location and clearly seen in the MMP velocity record did not cause any distortion of the interfacial θ and S gradients. A good example is

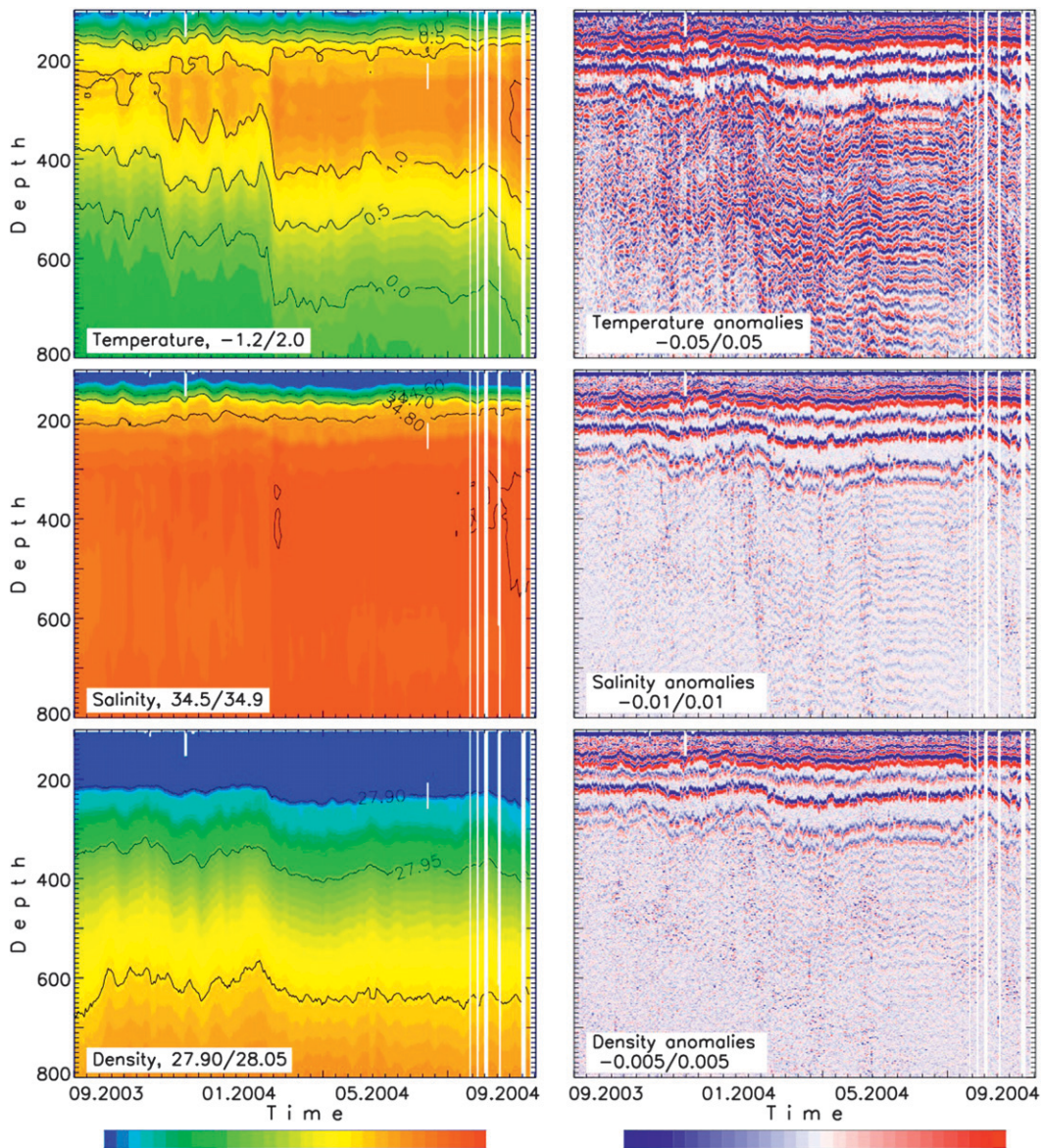


FIG. 2. Depth (vertical; m) vs time (horizontal) sections of (left) potential temperature ($^{\circ}$ C), salinity (psu), and potential density (σ_o , kg m^{-3}) and (right) their anomalies from the 2003–04 MMP record. Anomalies are computed relative to vertical means defined within a 3-m running window. White segments identify pieces of the record with missing data. The ranges of means and anomalies used for color maps are shown in white inserted windows within each panel.

provided by an event recorded at the mooring site in late December 2003 to early January 2004. During the event, both zonal and meridional velocity components changed their signs, consistent with its interpretation as an eddy. In the core of this event, the two shallowest interfaces deepened by ~ 15 m; however, after the event, the interfaces assumed their original depth (Fig. 6). During this event, the vertical gradients of θ and S across the interfaces were not changed. This is in contrast to what was observed in the Canada Basin, where a staircase structure was absent in

several θ and S profiles, presumably because of eddy activity (Timmermans et al. 2008).

c. Staircase structure above and below the AW core

Despite the apparent similarity between the six identified persistent interfaces, there is a substantial difference between the two sections of the thermohaline staircase above and below the AW core (Fig. 4, green line). Above the AW core (defined by the maximum temperature at ~ 250 – 290 m) where cold, freshwater

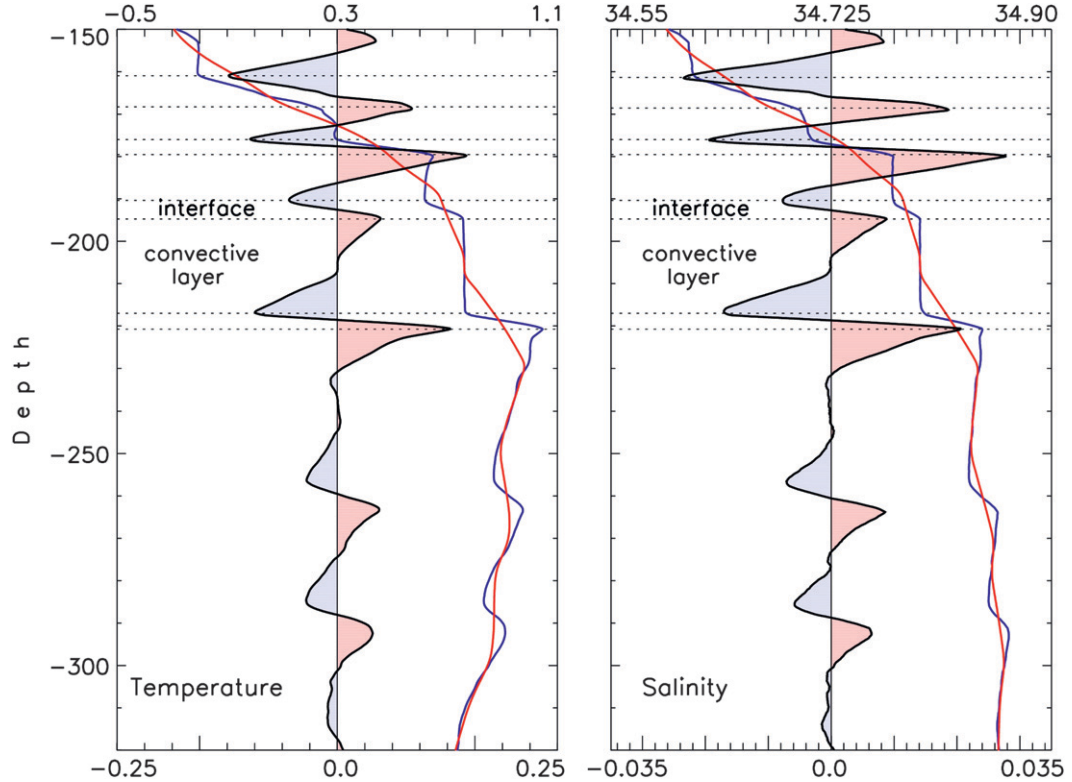


FIG. 3. One profile of potential temperature and salinity used to illustrate the method of selecting DL boundaries. Blue lines show original MMP profiles, red lines show vertical profiles smoothed with a 3-m window, and black lines with blue/red shades show their differences (anomalies). Peaks of these anomalies correspond to the upper and lower ends of the interfaces and convective layers. Horizontal dotted lines show four selected strong-gradient interfaces as an example. Note that two different scales for means (upper axes) and anomalies (lower axes) are used for the horizontal axes.

overlies warm, salty water, the interfaces separate nearly homogeneous layers (see Fig. 3). Based on prior studies, we assume that the layers are mixed by convection arising from differential diffusion at the edges of the DL interfaces (see, e.g., Turner 1973; Kelley 1984; Padman and Dillon 1987). We will refer to these layers as “convective layers.” The water column below the AW core, although stably stratified in σ_θ , exhibits thermohaline intrusions in which the depth intervals between identified interfaces are not homogeneous but instead show weak gradients of θ and S (both decreasing with depth). This intrusive structure suggests that the “salt fingering” mode of double diffusion (Stern 1960; Turner 1973; Kunze 2003; Schmitt 1995, 2003) may play a role in diapycnal fluxes below the AW core. However, because our main interest is in the upward flux of AW heat toward the surface mixed layer, for the remainder of this paper we ignore the staircase below the AW core.

d. Diffusive layering staircase characteristics

More than 300 daily samples of each interface’s upper and lower boundaries and corresponding steps in θ , S ,

and σ_θ derived from the MMP’s 2003–04 record provide a solid statistical basis for describing mean staircase characteristics. We first calculated the thickness of the convective layers H_l and interfaces h_i ; thickness is one of the basic characteristics of diffusive staircases (e.g., Kelley 1984). The temporal mean of various quantities describing each interface (Fig. 7) suggest that, on average, the interface thickness h_i was about 2–4 m. According to these estimates, the thickest interface was the shallowest and was centered at ~158-m depth (Fig. 7). These values of interface thickness are much greater than typical values of h_i in microstructure profiles through demonstrably active DL interfaces (see, e.g., Padman and Dillon 1987; Robertson et al. 1995), raising some doubt that the diffusive instability is presently active (cf. Howard et al. 2004). For the remainder of this paper, however, we will assume that these are DL interfaces whose thicknesses imply that (i) the interfaces are no longer active (in a double-diffusive sense); (ii) shear associated with other processes is interacting with the DL instability (Padman 1994); or (iii) some broadening is associated with the mechanics and response characteristics of the MMP

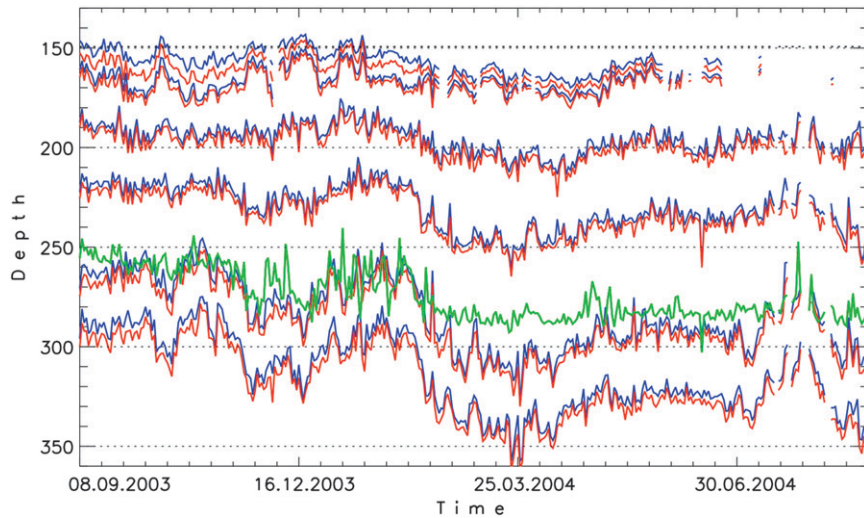


FIG. 4. Time series of depth of six staircase interfaces. Blue lines show upper boundaries and red lines show lower boundaries of the interfaces. Gaps in time series identifying the upper two interfaces are generally caused by merging and reemerging of the interfaces; gaps in the lower interfaces are due to errors in the temperature and/or salinity profiles. The upper four interfaces above the AW core defined by the depth of maximum temperature (green line) are selected as diffusive interfaces for the analysis.

sampling. We will discuss the implications of each of these possibilities as necessary below.

All interfaces were thicker before the first warm pulse passed through the mooring location in February 2004; however, the decrease of h_i in the uppermost interface was the most substantial. For example, this thickness was $\sim 5\text{--}6$ m during the first several months of the record and decreased to ~ 3 m after February 2004 (cf. a thickness change from ~ 3 to ~ 2 m in the neighboring interface centered at 167 m). Even after the warming event, the shallowest interface was thicker than the other layers. The reason for this nonmonotonic distribution of interface thickness with depth requires further investigation but may be related to vertical variability of shear associated with the mean flow and baroclinic tides.

The relative roles of temperature and salinity stratification in double diffusion are expressed by the density ratio (or “Turner number”) $R_\rho = (\beta \partial S / \partial z) / (\alpha \partial \theta / \partial z)$, where α is the thermal expansion coefficient and β is the haline contraction coefficient (both positive). The Turner number represents the contribution to the total buoyancy gradient from $\alpha \partial S / \partial z$ and $\beta \partial \theta / \partial z$; for the DL case in which salinity stratification dominates density changes, $R_\rho > 1$. As R_ρ approaches unity from above, the DL instability becomes more energetic because the intrinsically unstable temperature gradient through interfaces leads to more active convection in the adjacent convective layers (see Padman and Dillon 1987; Fernando 1989).

In the Arctic Ocean, typical values of R_ρ in regions where DL staircases occur range from ~ 2 in the Eurasian Basin north of Svalbard (Perkin and Lewis 1984; Kelley 1984) to 4–6 in the Beaufort Sea (Padman and Dillon 1987) and 2–7 in the Canada Basin (Timmermans et al.

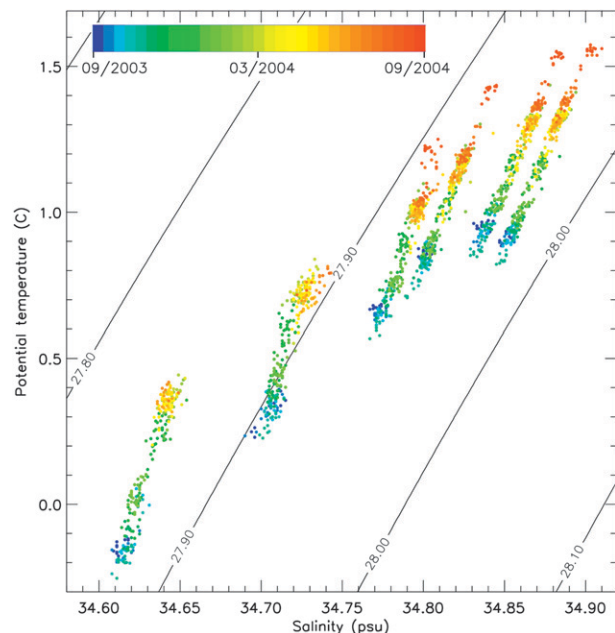


FIG. 5. Potential temperature–salinity ($^{\circ}$ C and psu, respectively) plot for the six interfaces identified in Figs. 2 and 4. Colors show time.

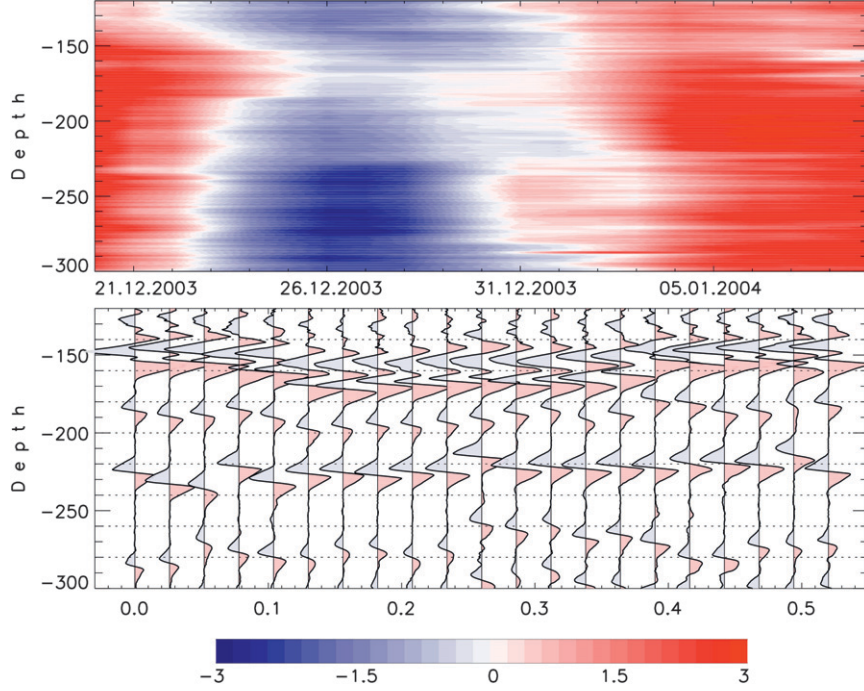


FIG. 6. (top) Anomalies of the zonal horizontal velocity component (cm s^{-1}) showing an eddy-like feature passing through the M1 mooring location in late December 2003–early January 2004. (bottom) Associated displacement of isopycnal surfaces as demonstrated by the change of salinity anomaly depths seen in daily profiles. Neighboring profiles are separated by 0.026.

2008). The mean values of R_p for the four DL interfaces identified in this study vary from 1.7 to 2.7 without a clear dependence of R_p on depth (Fig. 7). The probability distribution functions (PDFs) of R_p have modal values close to R_p means.

4. Heat fluxes

a. Methods for estimating DL heat fluxes

The most accurate method for estimating heat flux in a DL staircase is to measure the buoyancy flux within the high-gradient interfaces from microstructure profiles of scalar gradients ($\partial S/\partial z$ and $\partial\theta/\partial z$). This method is, however, generally impractical because of the very small length scales that must be resolved, especially for $\partial S/\partial z$ (Washburn et al. 1996). An alternative method relies on measuring velocity shear ($\partial u/\partial z$), calculating the dissipation rate ε , assuming that buoyancy transport through the interface is related to ε , and assuming that the interfacial buoyancy flux is carried through the adjacent layers by convection (for examples of this approach, see Padman and Dillon 1987; Lenn et al. 2009).

In the absence of microstructure data, however, heat flux F_h through a DL interface may be estimated using

laboratory-derived flux laws (e.g., Kelley 1984, 1990; Kelley et al. 2003) in which heat flux is given by the product of an empirically derived function of R_p and the change of potential temperature across the diffusive interface $\delta\theta$ to the $4/3$ power. Kelley (1990) proposed the following relationship:

$$F_h = 0.0032 e^{4.8/R_p^{0.72}} \rho c_p \left(\frac{g k_T \alpha}{\text{Pr}} \right)^{1/3} (\delta\theta)^{4/3}, \quad (1)$$

where $c_p = 4190 \text{ J kg}^{-1} \text{ }^{\circ}\text{C}^{-1}$ is specific heat of water, ρ is water density (kg m^{-3}), $g = 9.8 \text{ m s}^{-2}$ is acceleration due to gravity, $\text{Pr} = \nu/k_T$ is the Prandtl number, $\nu = 1.8 \times 10^{-6} \text{ m}^2 \text{ s}^{-1}$ is the kinematic viscosity, and $k_T = 1.4 \times 10^{-7} \text{ m}^2 \text{ s}^{-1}$ is the molecular diffusivity of heat (Kelley 1984). An alternative flux law was developed earlier by Marmorino and Caldwell (1976),

$$F_h = 0.00859 e^{4.6 \exp[-0.54(R_p - 1)]} \rho c_p \left(\frac{g k_T \alpha}{\text{Pr}} \right)^{1/3} (\delta\theta)^{4/3}. \quad (2)$$

Kelley (1990) noted that comparisons of Eqs. (1) and (2) to experimental data support the superiority of Eq. (1); however, the two models differ only in the dependence

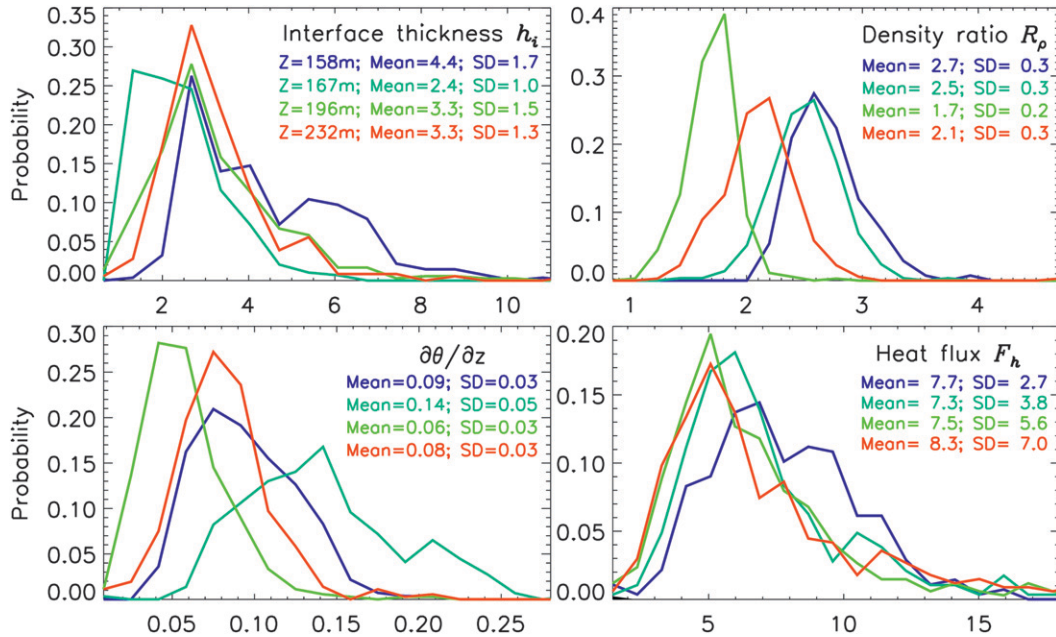


FIG. 7. Estimates of PDFs for the interface thickness h_i (m), the dimensionless density ratio R_p , the potential temperature gradients $\partial\theta/\partial z$ ($^{\circ}\text{C m}^{-1}$) over the interfaces, and the heat flux across the interfaces F_h (W m^{-2}). Color convention is used (top left) as described (e.g., red color is used for the layer with the mean depth of 232 m). Vertical axes show probability and horizontal axes show parameter values.

on R_p . Other models were tested by Robertson et al. (1995); for typical values of R_p , the heat flux estimates between all flux laws vary by about a factor of two.

The preceding flux laws assume that $\delta\theta$ and R_p are measured for each interface. Kelley (1984) proposed another form for Eq. (1), based on large-scale gradients and layer height H_l , expressed as the effective diffusivity of heat K_T ($\text{m}^2 \text{s}^{-1}$) through the staircase. From the relationship $\delta\theta = (H_l + h_i)\langle\partial\theta/\partial z\rangle$ (where $\langle\partial\theta/\partial z\rangle$ is a background gradient of θ , smoothed over several steps), we evaluate F_h using the following expression:

$$F_h = \rho c_p K_T \frac{\partial\theta}{\partial z}, \quad (3)$$

where K_T is

$$K_T = 0.00859 e^{4.6 \exp[-0.54(R_p - 1)]} \frac{k_T G^{4/3}}{\text{Pr}^{1/3} (R_p - 1)^{1/3}}. \quad (4)$$

In Eq. (4), $G = H_l(N/k_T)^{1/2}$ is a scaled layer thickness and N is the Brunt–Väisälä frequency averaged over vertical scales greater than $(H_l + h_i)$. Equation (4) is appropriate for use in models that cannot resolve individual steps in a DL staircase but where H_l and G may be parameterized based on large-scale hydrographic gradients.

b. Estimates of DL heat fluxes from MMP data

Mean values of F_h estimated by Eq. (1) vary from 7.3 to 8.3 W m^{-2} (Fig. 7). These values are much larger than most previous estimates of DL fluxes in the Arctic Ocean and arise from the relatively large values of $\delta\theta$ at each interface (see Fig. 3) and the relatively low values of R_p . As we noted in section 3, the observed values of $h_i > 1 \text{ m}$ suggest that the DL instability is either no longer active or is influenced by some external process. For the observed values of $\partial\theta/\partial z \approx 0.1^\circ\text{C m}^{-1}$ (Fig. 7), the laminar heat flux through a typical interface is $\rho c_p k_T \partial\theta/\partial z \approx 0.06 \text{ W m}^{-2}$. That is, significant values of heat flux (e.g., $F_h > 1 \text{ W m}^{-2}$) at the time of the observation requires that the heat transport through the interface be turbulent rather than laminar. Linden and Shirtcliffe (1978) and later authors note that turbulent transport is observed for interfaces with $R_p < 2$: this is frequently the case for the two deepest DL interfaces but not for the shallower ones (Fig. 7). However, the addition of possibly intermittent velocity shear such as from the mean flow and/or tides may change the range of R_p over which turbulent interfacial transport occurs. Alternatively, the observed staircase may be a “relict” DL staircase that was previously active but has been disrupted, perhaps by shear. In further discussion, we assume that the estimated DL heat fluxes above represent an approximate upper bound of either the current or recent state of the DL staircase.

In Fig. 8, we compare various pairs of double-diffusive parameters to further characterize the DL staircase. As expected from Eq. (1), F_h decreases with increasing R_ρ so that, for example, at $R_\rho > 3$ the heat fluxes are much suppressed compared with heat fluxes at lower density ratio R_ρ (Fig. 8a) (cf. Linden and Shirtcliffe 1978; Kelley 1984). Because F_h is calculated from Eq. (1), the scatter in F_h at each value of R_ρ represents the variability of $\delta\theta$. Similarly, F_h increases with $\delta\theta$ (Fig. 8b), with the scatter now arising from variability in R_ρ . The mean value of F_h is relatively uniform with vertical distance from the AW core (Fig. 7), suggesting little vertical heat flux divergence to explain cooling of the upper AW in the boundary current. Thus, although DL may be an effective process for moving heat from the AW core to the lower halocline, cooling of the upper AW layer itself requires that some other process such as lateral mixing is also active.

Although the values of F_h averaged over each interface are similar, there is substantial temporal variability of F_h as seen in Figs. 8a,b; the estimated standard deviations (SDs) are $\sim 2.7\text{--}7.0 \text{ W m}^{-2}$ (Fig. 7). Time series of the computed F_h corroborate this conclusion, showing large variations of estimated F_h at various time scales (Fig. 9). Particularly noticeable is a yearlong decreasing trend in F_h for the uppermost interface; F_h decreased from $5\text{--}6 \text{ W m}^{-2}$ to less than 2 W m^{-2} . However, estimated fluxes up to $\sim 10 \text{ W m}^{-2}$ were found across the deeper interfaces at the end of the record. We found no significant change of heat fluxes at the time of the eddy-like velocity perturbation (Figs. 6, 9); there is also no correlation between the two episodic warming events in February and late August 2004 and heat flux (Figs. 5 and 9).

c. Sensitivity of heat flux estimates to flux law formulation

The sensitivity of the computed F_h estimates to the choice of double-diffusive flux law formulation [Eqs. (1)–(4)] was evaluated. Estimates of means of F_h based on Eq. (2) were higher than values derived from Eq. (1) by 40%–55%, with greater differences in the deeper interfaces where modal values of R_ρ are smallest. Standard deviations varied from 47% for the shallowest layer to 59%–60% for the two deepest interfaces. These results are consistent with those presented by Robertson et al. (1995) for analyses of Weddell Sea microstructure data and follow from the ratio of the two equations' dependencies on R_ρ . Estimates of effective diffusivity K_T and F_h based on bulk stratification parameters [Eqs. (3) and (4)] and those from analyses of individual interfaces [Eq. (1)] were practically identical, as expected from their functional interdependence. Small differences arise through averaging because of the nonlinear influence of the $4/3$ power dependence on $\delta\theta$. The parameterized value of K_T is

a strong function of R_ρ (Fig. 8d) with values up to $\sim 2 \times 10^{-4} \text{ m}^2 \text{ s}^{-1}$, comparable to the values measured by Padman and Dillon (1991) over the Yermak Plateau and associated in that case with shear instability of baroclinic tides.

5. Discussion

Our estimates of K_T and F_h through the DL staircase above the AW core, presented in the previous section, assume that the flux laws proposed by Kelley (1990) apply to our data. The fits shown in Figs. 8a,b,d do not provide independent evidence of these flux laws because they are based on Eq. (1). Nevertheless, determining whether there are some universal relationships that allow DL fluxes to be represented in models is valuable. In this section, we discuss “independent” tests of the universality of DL staircase structure, the possible role of externally imposed shear (from, e.g., mean flow and baroclinic tides), and comparisons with nearby but nonsynoptic microstructure-based estimates of heat flux.

a. Relationships between key DL parameters

The principal requirement for DL flux parameterizations of diapycnal transport in ocean models is an estimate of $\delta\theta$ across the interface, because R_ρ across each interface is approximately given by R_ρ based on large-scale, model-resolved hydrographic gradients. The temperature step is given by $\delta\theta = (H_l + h_i)\langle\partial\theta/\partial z\rangle$, where H_l is usually much greater than h_i ; thus, if we can find a functional relationship between H_l and the large-scale stratification, we can parameterize $\delta\theta$, K_T , and F_h .

In Fig. 8c, we show dimensionless layer thickness G (see section 4b) as a function of R_ρ . The relationship between G and R_ρ used by Kelley (1984) for parameterizing the diffusivities (updated by Kelley et al. 2003) is based on the $1/4$ power law for $G(R_\rho)$. Our mean value of G ($\sim 10^3$) is about 1–3 times greater than those reported by Kelley et al. (2003) for staircases with similar R_ρ . We found that the 0.255 power law is the best fit to our observational data (shown in Fig. 8c). However, our observations show a very noisy relationship with a low (albeit statistically significant) correlation of $R = 0.31$. Our tentative conclusion is that there is roughly a factor of 3 uncertainty in G (and therefore also in H_l).

Kelley (1984) suggests that the layer Rayleigh number $\text{Ra} = \alpha g \Delta \theta H_l^{3/2} / (\nu k_T)$ (i.e., representing a ratio of buoyancy forces and diffusion in the convecting layers) correlates with R_ρ , increasing roughly linearly with R_ρ (see his Fig. 3). In contrast, we find a strong inverse dependence (Fig. 8e) and much higher values of Ra than reported by Kelley (1984), consistent with our typically much larger values of G . We do not have an explanation

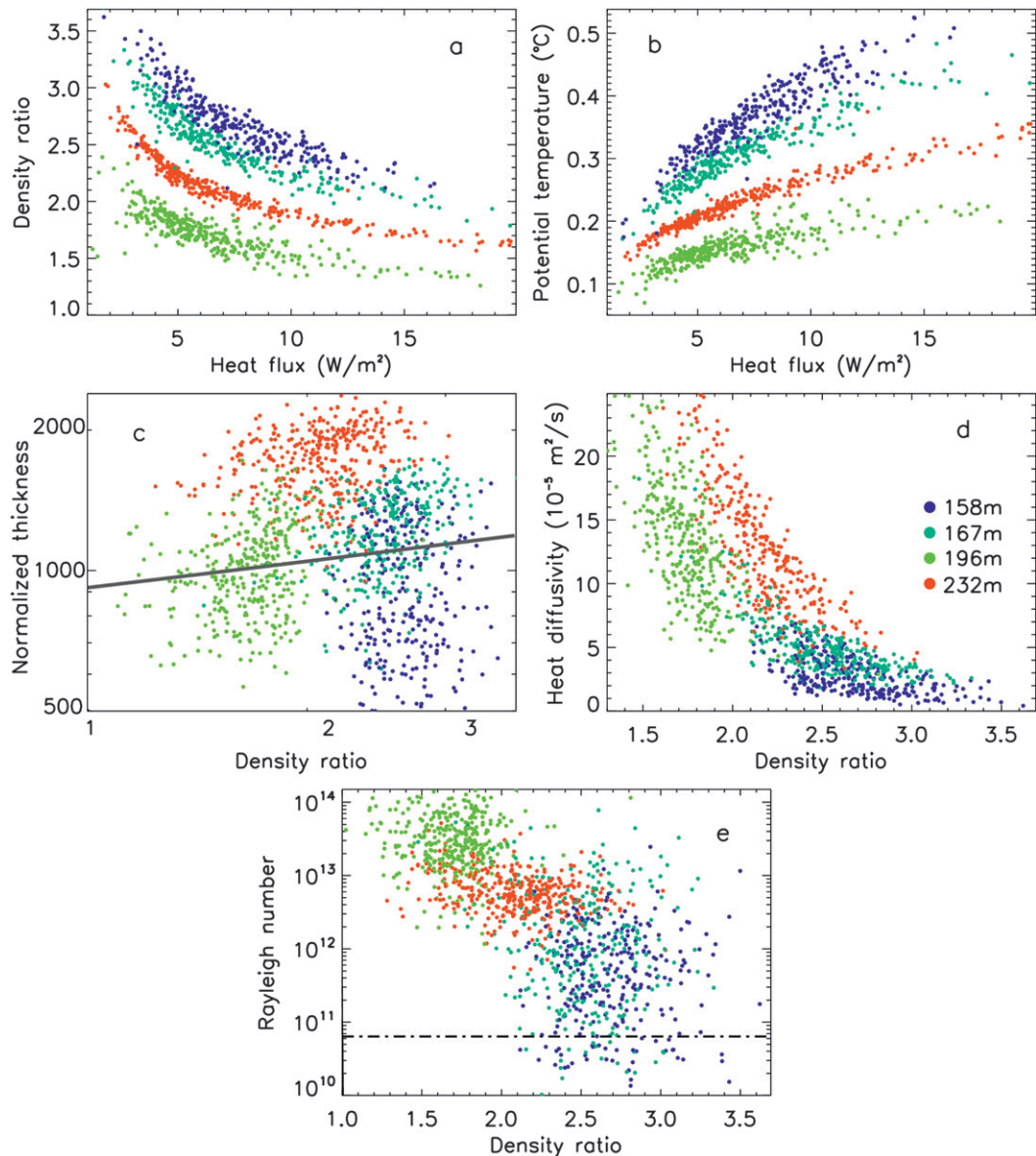


FIG. 8. Relationship between key double-diffusive parameters: (a) the dimensionless density ratio R_ρ vs heat flux across the interface F_h , (b) potential temperature step $\delta\theta$ across the interfaces vs F_h , (c) dimensionless normalized thickness of the layers G vs R_ρ [log scales are used; the solid curve results from using the $1/4$ power law for $G(R_\rho)$], (d) the effective diffusivity of heat K_T vs R_ρ , and (e) Rayleigh number Ra (log scale is used) vs R_ρ . Dashed-dotted line in (e) shows critical value for Ra , above which layers should be fully turbulent. Color key is shown in (d).

for this discrepancy. The relationships shown in Figs. 8c,e may indicate the significant influence of other processes on the DL instability in the region of our mooring and imply the need for more detailed measurements in this region to help improve parameterizations of DL-driven K_T and F_h for use in regional and global ocean models.

b. Potential impact of velocity shear on heat fluxes

The flux laws, being based on idealized experiments in laboratory tanks, do not capture the possible interaction

between double-diffusive processes and other sources of ocean variability such as shear associated with internal waves. Padman (1994) proposed that nonlinear interaction between velocity shear and double-diffusive convection might significantly increase the heat, salt, and momentum fluxes through a DL staircase. If this is true, we would expect the mechanism to be most important along the Arctic continental slope regions where shears are expected to be large relative to those in the deep basins (Padman 1995) because of mean flow and strong

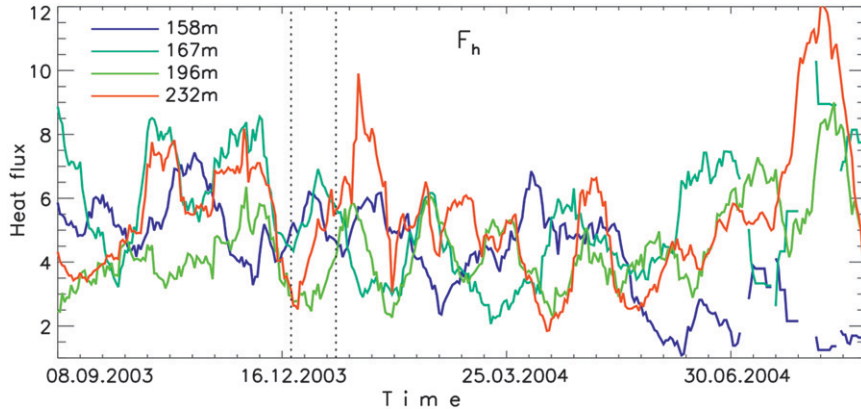


FIG. 9. 15-day running mean time series of the heat fluxes F_h (W m^{-2}) across the four interfaces. Vertical dotted lines show the segment of the record with the eddy shown in Fig. 6.

tidal currents (Padman and Erofeeva 2004). We tested the importance of velocity shear $\partial \mathbf{U} / \partial z$ using our dataset, focusing on the 150–350-m depth range and a selected segment of the annual record during which the interfaces were almost horizontal (Fig. 10). Maximal density anomalies are aligned along the double-diffusive interfaces. Current speed anomalies and shear squared ($\partial \mathbf{U} / \partial z$)² are noisy; nevertheless, the record demonstrates that the shear is largest across the interfaces. Averaged over the selected time interval, the Richardson number $Ri = N^2 / (\partial \mathbf{U} / \partial z)^2$ is always greater than $1/4$, suggesting that enhanced velocity shear is usually not sufficient to overcome the effects of buoyancy in the diffusive interfaces. This is consistent with the suggestion by Melling et al. (1984) that double-diffusive layers are only found when shear is too weak to disrupt the staircase through shear instabilities. Thus, we tentatively conclude that, at the mooring location, the laboratory-derived double-diffusive laws for unsheared steps are valid for estimates of DL heat fluxes. However, it is possible that the interaction of shear with the DL instability is manifested through the observed thick interfaces, with h_i set by shear that is intensified across interfaces by convection in the adjacent layers driven by the DL instability (Padman 1994). For the vast upstream areas of the Eurasian Basin where the currents (and presumably shear) are strong (Schauer et al. 2004, 2008; Ivanov et al. 2009), the interaction between double diffusion and shear may play an even stronger role in setting the net diapycnal fluxes.

c. Comparison of heat flux estimates based on flux laws and microstructure data

The preceding analyses are necessarily limited by a lack of direct measurements of K_T and F_h . We have no concrete evidence (i.e., direct turbulence measurements) that the DL fluxes are sufficiently large to play a significant role

in transporting AW heat to the upper ocean at the location of our mooring. However, the estimated double-diffusive heat fluxes of $6\text{--}8 \text{ W m}^{-2}$ are roughly consistent with the estimates of downstream heat content changes in the AW and overlying layer based on CTD profiles over the Laptev Sea slope, which yield $\sim 3\text{--}4 \text{ W m}^{-2}$ for the early 2000s and up to $\sim 6 \text{ W m}^{-2}$ for the peak warming year of 2007 (Polyakov et al. 2011). Microstructure observations have shown, however, that halocline mixing in the Arctic interior is weak, $< 1 \text{ W m}^{-2}$ (e.g., Rainville and Winsor 2008; Timmermans et al. 2008). Measured heat fluxes in the Beaufort Sea thermohaline staircase are $< 0.1 \text{ W m}^{-2}$ (Padman and Dillon 1987), although these are for steps with much smaller $\delta\theta$ and higher R_p than in the present dataset.

Our heat flux estimates can also be compared with those reported by Lenn et al. (2009), who analyzed microstructure profiles from three transects across the continental slope adjacent to the Laptev and East Siberian Seas. For one of these profiles, station 40 in the Makarov Basin, the high-resolution temperature profile shows a few interfaces with large $\delta\theta$ above the AW core (Fig. 11a), similar to profiles in our MMP dataset. We reanalyzed this profile by restricting the calculation to 1-s ($\sim 0.6 \text{ m}$) blocks of data for which the value of N^2 exceeded $0.2 \times 10^{-4} \text{ s}^{-2}$. For these blocks that, in general, correspond to the DL interfaces, we then estimated effective diffusivity from $K_T = \Gamma \epsilon / N^2$, where Γ is the mixing efficiency. Taking a typical value of $\Gamma = 0.2$, values of F_h through the large interfaces are on the order of 1 W m^{-2} (Fig. 11b). However, as Inoue et al. (2007) noted, the value of Γ for DL instabilities can be much higher than this, close to unity, because the source of shear variance is the buoyancy flux itself rather than buoyancy flux being the result of shear-generated turbulent kinetic energy working against a stable buoyancy gradient. If we use

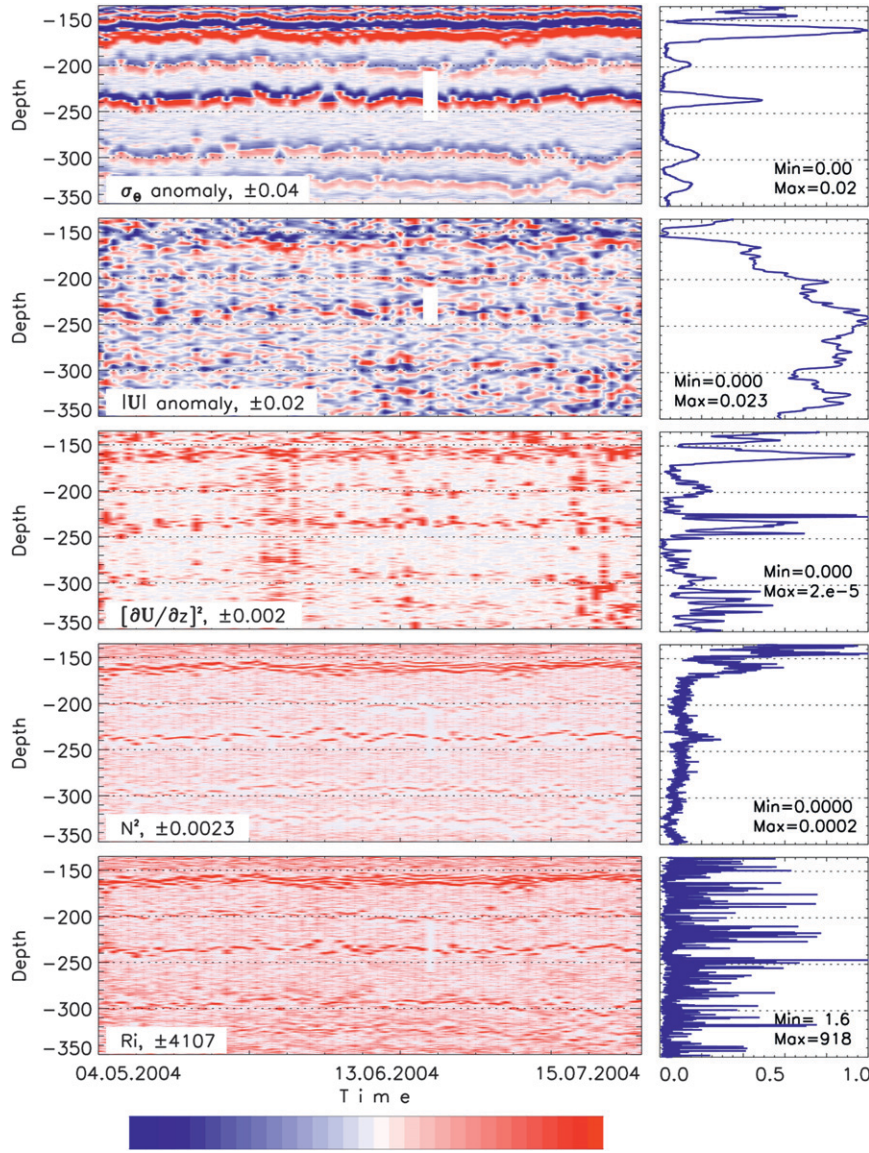


FIG. 10. (left) Depth (m) vs time sections of density σ_θ anomalies (kg m^{-3}), current speed $|U|$ anomalies (m s^{-1}), the squared velocity shear $(\partial U / \partial z)^2$ (s^{-2}), the squared Brunt–Väisälä frequency N^2 (s^{-2}), and the dimensionless Richardson number $Ri = N^2 / (\partial U / \partial z)^2$. (right) SDs of σ_θ and U and time-averaged estimates of $(\partial U / \partial z)^2$, N^2 , and Ri . All values in (right) are normalized using their minimum and maximum values in order to fit a 0–1 scale.

$\Gamma = 1$, the fluxes in Fig. 11b would be 5 times greater and generally close to the estimates based on application of the double-diffusive flux law given by Eq. (1) (see Fig. 11c). That is, the microstructure measurements using $\Gamma = 1$, DL flux laws applied to our mooring data, and the downstream evolution of AW core temperature all suggest upward heat fluxes of about 5 W m^{-2} for about 100 m above the AW core and implicate double diffusion as the primary source of this flux.

We cannot measure the buoyancy and heat transport through the convecting layers with presently available

datasets. However, the estimated values of Ra for the convective layers separating the diffusive staircases were high (Fig. 8e), exceeding (with only few exceptions) the critical value of $Ra = 64 \times 10^9$ for a boundary layer cooled from the top (Fedorov and Ginsburg 1992). This analysis suggests that these layers are fully turbulent, explaining the presence of numerous small-scale perturbations in the quasi-homogeneous layers seen in microstructure profiles (Fig. 12). It is usually assumed that the buoyancy (and heat) fluxes through the DL interfaces are balanced by the turbulent fluxes through the convectively

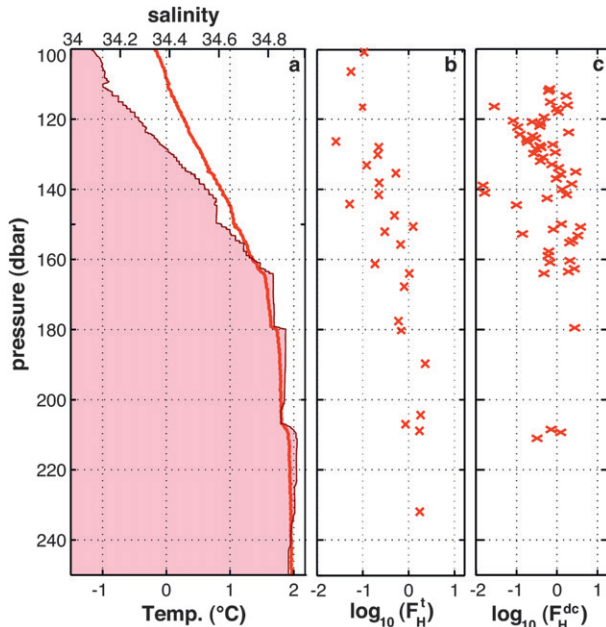


FIG. 11. Microstructure observations for a typical station from the Laptev Sea slope region. (a) Temperature is shown by shading and salinity is shown by the thick line. (b) Estimates of turbulent heat flux derived from microstructure measurements using $\Gamma = 0.2$ applied only to 2-s (~ 1.2 m) data blocks with $N^2 > 0.2 \times 10^{-4} \text{ s}^{-2}$ (see text). (c) Double-diffusive heat flux derived from microstructure measurements of temperature and salinity and the flux law given by Eq. (1). For further details, see Lenn et al. (2009). Horizontal axes in (b) and (c) use logarithmic scale.

forced layers, so that the heat fluxes of several W m^{-2} estimated at each interface represent a quasi-continuous upward flux through the entire staircase.

6. Concluding remarks

An MMP record more than one year long from the Laptev Sea continental slope demonstrates the existence of highly persistent staircase layering in the upper AW and lower halocline ($\sim 140\text{--}350$ -m depth range). These layers survive eddies, internal waves, tidal mixing (ongoing analysis), and even episodic warming events without substantial changes of their characteristics. Inferred diffusive heat fluxes across the upper four layers overlying the AW core are on the order of $6\text{--}8 \text{ W m}^{-2}$, significantly higher than prior estimates of upper-ocean heat fluxes in the Arctic Ocean interior but generally consistent with prior estimates based on downstream evolution of the AW core as it circulates eastward along the eastern Arctic Ocean continental slope. If these estimates are correct, double diffusion is an effective mechanism for transferring AW heat upward over more than a 100-m depth range toward the upper halocline. The inferred heat fluxes experience strong (up to several W m^{-2})

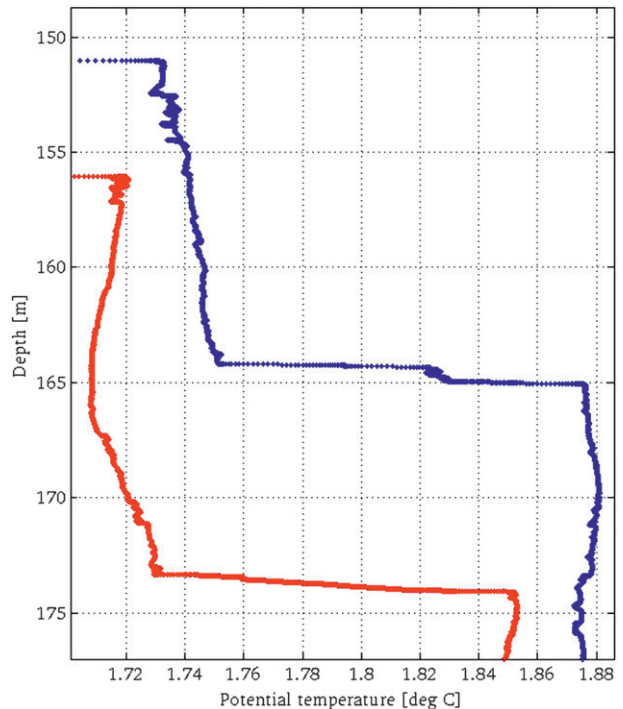


FIG. 12. Segments of two potential temperature profiles from microstructure measurements made during the 2007 Nansen and Amundsen Basins Observational System (NABOS) cruise over the Laptev Sea slope (red profile is measured at $78^{\circ}55'\text{N}, 125^{\circ}59'\text{E}$ and blue profile is measured at $79^{\circ}25'\text{N}, 126^{\circ}00'\text{E}$, which are 65 and 118 km from the mooring M1 site, respectively). Vertical resolution of these measurements is ~ 2 mm. Note that many pulsations are in vertically well-mixed (convective) layers; pulsations are not pronounced in interface layers with strong vertical gradients.

temporal variability at different time scales resolved by the available record of roughly daily profiles.

Many questions remain regarding the magnitude of the actual fluxes through the DL staircase and the mechanisms that maintain the staircase layering over time. Radko (2005, 2007) suggested that equilibration of the layers may result from a delicate balance of buoyancy forces between the interface and convective layers. We are particularly interested in the hypothesis that the presence of background velocity shear, associated with the boundary flow of AW, tides, and other internal waves, might significantly increase the diapycnal fluxes (Padman 1994). The MMP record of currents (even though it is very noisy) shows the existence of the layer structure in the currents, with shear focused at the DL interfaces (Fig. 10); however, these data are too poorly resolved to test our hypothesis at this time.

Assuming that our estimates of DL fluxes over the AW core are approximately correct, the DL instability is a critical process determining the hydrographic variability of the Arctic Ocean above the AW layer. The modeled

sensitivity of DL heat fluxes to hydrographic variability represented by N and R_p , the possibility that interactions with velocity shear can determine whether DL is active, and the magnitude of the associated fluxes indicate that models of Arctic Ocean state need to include explicit representation of the DL instability. However, we note that present datasets are inadequate for validating parameterizations of DL fluxes along the eastern Arctic margins, requiring further studies focused on the DL instability in this region.

Finally, we note that the magnitude and uncertainty of our inferred DL fluxes are large relative to the heat budget imbalance explaining changes of the Arctic Ocean sea ice cover during the past several decades (Kwok and Untersteiner 2011). If a mechanism exists to transport the heat flux from the lower halocline to the surface mixed layer, changing the predicted values of DL fluxes from the AW up to the lower halocline within the present range of uncertainty could change the sign of the time-averaged heat budget experienced by the sea ice. Given the importance of sea ice in evolution of Arctic climate, further improving our understanding of the contribution of the DL instability to upper-ocean fluxes is critical.

Acknowledgments. This study was supported by JAMSTEC (IP, RR, and VI), NOAA (IP), NSF (IP and LP), NASA (AP, IP, and LP) and UK (YL) grants. We acknowledge help of R. Bekryaev in the analysis of fitness of power laws to our observational data. We thank S. Kirillov for careful reading of the early version of our manuscript, which resulted in finding a bug in the data processing. We thank an anonymous reviewer for helpful suggestions.

REFERENCES

- Aagaard, K., 1989: A synthesis of the Arctic Ocean circulation. *Rapp. P.-V. Reun. Cons. Int. Explor. Mer*, **188**, 11–22.
- Carmack, E. C., R. W. Macdonald, R. G. Perkin, F. A. McLaughlin, and R. J. Pearson, 1995: Evidence for warming of Atlantic water in the Southern Canadian Basin of the Arctic Ocean: Results from the Larsen-93 expedition. *Geophys. Res. Lett.*, **22**, 1061–1064.
- Dmitrenko, I. A., and Coauthors, 2008: Toward a warmer Arctic Ocean: Spreading of the early 21st century Atlantic Water warm anomaly along the Eurasian Basin margins. *J. Geophys. Res.*, **113**, C05023, doi:10.1029/2007JC004158.
- Fedorov, K. N., and A. I. Ginsburg, 1992: *The Near-Surface Layer of the Ocean*. VSP, 259 pp.
- Fer, I., 2009: Weak vertical diffusion allows maintenance of cold halocline in the central Arctic. *Atmos. Oceanic Sci. Lett.*, **2**, 148–152.
- Fernando, H. J. S., 1989: Oceanographic implications of laboratory experiments on diffusive interfaces. *J. Phys. Oceanogr.*, **19**, 1707–1715.
- Howard, S. L., J. Hyatt, and L. Padman, 2004: Mixing in the pycnocline over the western Antarctic Peninsula shelf during Southern Ocean GLOBEC. *Deep-Sea Res. II*, **51**, 1965, doi:10.1016/j.dsr2.2004.08.002.
- Inoue, R., H. Yamazaki, F. Wolk, T. Kono, and J. Yoshida, 2007: An estimation of buoyancy flux for a mixture of turbulence and double diffusion. *J. Phys. Oceanogr.*, **37**, 611–623.
- Ivanov, V. V., and Coauthors, 2009: Seasonal variability in Atlantic Water off Spitsbergen. *Deep-Sea Res. I*, **56**, 1–14.
- Kelley, D., 1984: Effective diffusivities within oceanic thermohaline staircases. *J. Geophys. Res.*, **89** (C6), 10 484–10 488.
- , 1990: Fluxes through diffusive staircases: A new formulation. *J. Geophys. Res.*, **95**, 3365–3371.
- , H. J. S. Fernando, A. E. Gargett, J. Tanny, and E. Özsoy, 2003: The diffusive regime of double-diffusive convection. *Prog. Oceanogr.*, **56**, 461–481.
- Krishfield, R. A., and D. K. Perovich, 2005: Spatial and temporal variability of oceanic heat flux to the Arctic ice pack. *J. Geophys. Res.*, **110**, C07021, doi:10.1029/2004JC002293.
- Kunze, E., 2003: A review of oceanic salt fingering theory. *Prog. Oceanogr.*, **56**, 399–417.
- Kwok, R., and N. Untersteiner, 2011: The thinning of Arctic sea ice. *Phys. Today*, **64**, 36–41.
- Lenn, Y.-D., and Coauthors, 2009: Vertical mixing at intermediate depths in the Arctic boundary current. *Geophys. Res. Lett.*, **36**, L05601, doi:10.1029/2008GL036792.
- Linden, P. F., and T. G. L. Shirtcliffe, 1978: The diffusive interface in double diffusive convection. *J. Fluid Mech.*, **87**, 417–432.
- Marmorino, G. O., and D. R. Caldwell, 1976: Heat and salt transport through a diffusive thermohaline interface. *Deep-Sea Res.*, **23**, 59–67.
- Martinson, D. G., and M. Steele, 2001: Future of the Arctic sea ice cover: Implications of an Antarctic analog. *Geophys. Res. Lett.*, **28**, 307–310.
- Maykut, G. A., and M. G. McPhee, 1995: Solar heating of the Arctic mixed layer. *J. Geophys. Res.*, **100**, 24 691–24 703.
- McPhee, M. G., T. Kikuchi, J. H. Morison, and T. P. Stanton, 2003: Ocean-to-ice heat flux at the North Pole environmental observatory. *Geophys. Res. Lett.*, **30**, 2274, doi:10.1029/2003GL018580.
- Melling, H., R. A. Lake, D. R. Topham, and D. B. Fissel, 1984: Oceanic thermal structure in the western Canadian Arctic. *Cont. Shelf Res.*, **3**, 233–258.
- Padman, L., 1994: Momentum fluxes through sheared oceanic thermohaline steps. *J. Geophys. Res.*, **99**, 22 491–22 499.
- , 1995: Small-scale physical processes in the Arctic Ocean. *Arctic Oceanography: Marginal Ice Zones and Continental Shelves*, W. O. Smith and J. M. Grebmeier, Eds., Coastal and Estuarine Studies, Vol. 49, Smith, Amer. Geophys. Union, 97–129.
- , and T. M. Dillon, 1987: Vertical heat fluxes through the Beaufort Sea thermohaline staircase. *J. Geophys. Res.*, **92** (C10), 10 799–10 806.
- , and —, 1989: Thermal microstructure and internal waves in the Canada Basin diffusive staircase. *Deep-Sea Res.*, **36A**, 531–542.
- , and —, 1991: Turbulent mixing near the Yermak Plateau during the Coordinated Eastern Arctic Experiment. *J. Geophys. Res.*, **96** (C3), 4769–4782.
- , and S. Erofeeva, 2004: A barotropic inverse tidal model for the Arctic Ocean. *Geophys. Res. Lett.*, **31**, L02303, doi:10.1029/2003GL019003.
- Perkin, R. G., and E. L. Lewis, 1984: Mixing in the West Spitsbergen Current. *J. Phys. Oceanogr.*, **14**, 1315–1325.
- Perovich, D. K., B. Light, H. Eicken, K. F. Jones, K. Runciman, and S. V. Nghiem, 2007: Increasing solar heating of the Arctic Ocean and adjacent seas, 1979–2005: Attribution and role in

- the ice-albedo feedback. *Geophys. Res. Lett.*, **34**, L19505, doi:10.1029/2007GL031480.
- , J. A. Richter-Menge, K. F. Jones, and B. Light, 2008: Sunlight, water, and ice: Extreme Arctic sea ice melt during the summer of 2007. *Geophys. Res. Lett.*, **35**, L11501, doi:10.1029/2008GL034007.
- Polyakov, I. V., and Coauthors, 2005: One more step toward a warmer Arctic. *Geophys. Res. Lett.*, **32**, L17605, doi:10.1029/2005GL023740.
- , and Coauthors, 2010: Arctic Ocean warming contributes to reduced polar ice cap. *J. Phys. Oceanogr.*, **40**, 2743–2756.
- , and Coauthors, 2011: Fate of early 2000s Arctic warm water pulse. *Bull. Amer. Meteor. Soc.*, **92**, 561–566.
- Quadfasel, D. A., A. Sy, D. Wells, and A. Tunik, 1991: Warming in the Arctic. *Nature*, **350**, 385.
- Radko, T., 2005: What determines the thickness of layers in a thermohaline staircase? *J. Fluid Mech.*, **523**, 79–98.
- , 2007: Mechanics of merging events for a series of layers in a stratified turbulent fluid. *J. Fluid Mech.*, **577**, 251–273.
- Rainville, L., and P. Winsor, 2008: Mixing across the Arctic Ocean: Microstructure observations during the Beringia 2005 Expedition. *Geophys. Res. Lett.*, **35**, L08606, doi:10.1029/2008GL033532.
- Robertson, R., L. Padman, and M. D. Levine, 1995: Fine structure, microstructure, and vertical mixing processes in the upper ocean in the western Weddell Sea. *J. Geophys. Res.*, **100** (C9), 18 517–18 535.
- Rudels, B., E. P. Jones, L. G. Anderson, and G. Kattner, 1994: On the intermediate depth waters of the Arctic Ocean. *The Polar Oceans and Their Role in Shaping the Global Environment: The Nansen Centennial Volume*, *Geophys. Monogr.*, Vol. 85, Amer. Geophys. Union, 33–46.
- , L. G. Anderson, and E. P. Jones, 1996: Formation and evolution of the surface mixed layer and halocline of the Arctic Ocean. *J. Geophys. Res.*, **101**, 8807–8821.
- Schauer, U., E. Fahrbach, S. Osterhus, and G. Rohardt, 2004: Arctic warming through the Fram Strait: Oceanic heat transport from 3 years of measurements. *J. Geophys. Res.*, **109**, C06026, doi:10.1029/2003JC001823.
- , A. Beszczynska-Möller, W. Walczowski, E. Fahrbach, J. Piechura, and E. Hansen, 2008: Variation of flow through the Fram Strait to the Arctic Ocean between 1997 and 2006. *Arctic–Subarctic Ocean Fluxes*, B. Dickson, J. Meincke, and P. Rhines, Eds., Springer, 65–85.
- Schmitt, R. W., 1995: The salt finger experiments of Jevons (1857) and Rayleigh (1880). *J. Phys. Oceanogr.*, **25**, 8–17.
- , 2003: Observational and laboratory insights into salt finger convection. *Prog. Oceanogr.*, **56** (3–4), 419–433.
- Shaw, W. J., T. P. Stanton, M. G. McPhee, J. H. Morison, and D. G. Martinson, 2009: Role of the upper ocean in the energy budget of Arctic sea ice during SHEBA. *J. Geophys. Res.*, **114**, C06012, doi:10.1029/2008JC004991.
- Sirevaag, A., and I. Fer, 2009: Early spring oceanic heat fluxes and mixing observed from drift stations north of Svalbard. *J. Phys. Oceanogr.*, **39**, 3049–3069.
- Steele, M., and T. Boyd, 1998: Retreat of the cold halocline layer in the Arctic Ocean. *J. Geophys. Res.*, **103**, 10 419–10 435.
- Stern, M. E., 1960: The ‘salt-fountain’ and thermohaline convection. *Tellus*, **2**, 172–175.
- Timmermans, M.-L., J. Toole, R. Krishfield, and P. Winsor, 2008: Ice-Tethered Profiler observations of the double-diffusive staircase in the Canada Basin thermocline. *J. Geophys. Res.*, **113**, C00A02, doi:10.1029/2008JC004829.
- Toole, J. M., M.-L. Timmermans, D. K. Perovich, R. A. Krishfield, A. Proshutinsky, and J. A. Richter-Menge, 2010: Influences of the ocean surface mixed layer and thermohaline stratification on arctic sea ice in the central Canada Basin. *J. Geophys. Res.*, **115**, C10018, doi:10.1029/2009JC005660.
- Turner, J. S., 1973: *Buoyancy Effects in Fluids*. Cambridge University Press, 368 pp.
- Washburn, L., T. F. Duda, and D. C. Jacobs, 1996: Interpreting conductivity microstructure: Estimating the temperature variance dissipation rate. *J. Atmos. Oceanic Technol.*, **13**, 1166–1188.